SCIENCE CHINA
Chemistry

• ARTICLES •
• SPECIAL TOPIC • Chemical Challenges in Nuclear Fuel Cycle

November 2014 Vol.57 No.11: 1449–1458
doi: 10.1007/s11426-014-5195-7

Poly(amidoxime)-reduced graphene oxide composites as adsorbents for the enrichment of uranium from seawater

SHAO DaDong[1,2], LI JiaXing[1] & WANG XiangKe[1,2,3*]

[1]*School of Environment and Chemical Engineering, North China Electric Power University, Beijing 102206, China*
[2]*School for Radiological and Interdisciplinary Sciences, Soochow University, Suzhou 215123, China*
[3]*Collaborative Innovation Center of Radiation Medicine of Jiangsu Higher Education Institutions, China*

Received May 7, 2014; accepted July 8, 2014; published online September 24, 2014

The development of efficient materials for high extraction of uranium (UO_2^{2+}) from seawater is critical for nuclear energy. Poly(amidoxime)-reduced graphene oxide (PAO/rGO) composites with excellent adsorption capability for UO_2^{2+} were synthesized by *in situ* polymerization of acrylonitrile monomers on GO surfaces, followed by amidoximation treatment with hydroxylamine. The adsorption capacities of PAO/rGO composites for UO_2^{2+} reached as high as 872 mg/g at pH 4.0. The excellent tolerance of these composites for high salinity and their regeneration-reuse properties can be applied in the nuclear-fuel industry by high extraction of trace UO_2^{2+} ions from seawater.

uranium, amidoxime, graphene, acrylonitrile, adsorption

1 Introduction

Nuclear energy is regarded as a sustainable solution to the increasing problem of global energy, and uranium is one of the most essential and fundamental materials in the nuclear energy industry [1]. The long-term dependence on a sufficient uranium supply is a crucial and urgent issue. However, the known extractable reserves of uranium are limited and restricted to a few land places in the world. Furthermore, > 99% of global uranium exists primarily as UO_2^{2+} with an average concentration of ~3.0 μg/L in seawater [1].

Adsorption techniques are widely used as feasible and economic ways to achieve radionuclides preconcentration and extraction from aqueous solutions [2–9]. The high extraction of UO_2^{2+} from aqueous solution by adsorbents, such as oxide materials [10], carbon materials [2], and inorganic-organic composites [11] have been widely investigated. However, to our best knowledge, most reported natural and synthesized materials present the maximum adsorption capacities for UO_2^{2+} of 10–100 mg/g under general operation conditions. Furthermore, adsorption of UO_2^{2+} from seawater is restrained by the competitive adsorption of other coexisting cations [12]. Therefore, the development of adsorbents with high adsorption capacity for trace UO_2^{2+} in seawater is critical for the development of nuclear energy, and is currently one of the most important challenges for nuclear science and technology.

Graphene oxide (GO) has attracted significant interest in various fields due to its physicochemical properties. The high surface area (theoretically, ~2600 m^2/g) [13] and abundant oxygen-containing functional groups provide GO with potential adsorption capability for UO_2^{2+}. However, due to the lack of special binding sites for UO_2^{2+} on GO surfaces and its self-accumulation in aqueous solution, the maximum adsorption capacity of GO (27.6 mg/g, pH 5.0) [14] for UO_2^{2+} is even lower than that of carbon nanotubes (112 mg/g, pH 5.0) [2] and resins (120.3 mg/g, pH 5.5) [13] under similar operation conditions.

The adsorption process is controlled by the functional

*Corresponding author (email: xkwang@ipp.ac.cn; xkwang@suda.edu.cn)

groups on the adsorbent surface. The surface modification of GO with suitable functional groups would significantly enhance its adsorption capability for UO_2^{2+}. Therefore, the introduction of proper functional groups onto GO surfaces is crucial for its real application in the high extraction of UO_2^{2+} from seawater. Owing to its excellent affinity with UO_2^{2+}, amidoxime (AO) was widely accepted as one of the most promising binding sites for UO_2^{2+} due to its specific binding affinity with UO_2^{2+} [15–18]. For this reason, modification of the GO surface with AO would thought to result in the high extraction of UO_2^{2+} from seawater. As far as we know, GO's physicochemical properties and adsorption capability for UO_2^{2+} have not previously been studied.

We synthesized poly(amidoxime) on a GO surface by *in situ* polymerization of acrylonitrile monomers and followed by amidoximation treatment with hydroxylamine to convert acrylonitrile into poly(amidoxime) (denoted as PAO/rGO), and conducted a study to explore the adsorption capability of PAO/rGO composites for UO_2^{2+} under a variety of operation conditions. The results showed that PAO/rGO composites present exceptional performance in the high extraction of μg/L level UO_2^{2+} ions from seawater, which is crucial in nuclear fuel achievement.

2 Experimental

2.1 Synthesis of PAO/rGO composites

PAO/rGO composites with different PAO contents were prepared with *in situ* polymerization of acrylonitrile monomer on the GO surface in the presence of $(NH_4)_2S_2O_8$. We used NH_2OH for amidoximation and reduction [19, 20]. Briefly, acrylonitrile monomer (0.5–8.0 g/L) and GO (2 g/L), suspended in aqueous solutions (100 mL), were heated to 50 °C with stirring [17]. Equal molars of $(NH_4)_2S_2O_8$/ aqueous solution (0.1 mol/L) and the proper amount of Milli-Q water were added to achieve a total volume of 400 mL. The polymerizations of acrylonitrile monomer on GO surfaces were carried at 50 °C for 3 h. The suspensions were centrifuged and rinsed with a combination solution of 5:1 methanol-water and Milli-Q water to remove $(NH_4)_2S_2O_8$, acrylonitrile monomer, and poly(acrylonitrile) homopolymer. The derived poly(acrylonitrile)/GO materials were dispersed in 100 mL 66.5 g/L NH_2OH solution and amidoximated at 70 °C for 3 h [17]. After the centrifugation of the 5:1 methanol-water and Milli-Q water solutions, the derived products were oven dried at 50 °C for one week to obtain PAO/rGO composites. All acrylonitrile monomers were assumed to have been polymerized on GO surface; these were denoted as 0.25PAO/rGO, 0.5PAO/rGO, 1.0PAO/rGO, 2.0PAO/rGO, and 4.0PAO/rGO with respective weight ratios of PAO to rGO of 0.25:1, 0.5:1, 1:1, 2:1 and 4:1. The actual weight ratio of PAO to rGO in the PAO/rGO composites was measured by thermogravimetric analysis (TGA). We also prepared PAO and rGO by the same method to compare their adsorption capacities with the PAO/rGO composites.

2.2 Characterization of PAO/rGO composites

The physiochemical properties of PAO/rGO composites were studied and evaluated by scanning electron microscopy (SEM), Raman spectroscopy, X-ray photoelectron spectroscopy (XPS), and thermogravimetric analysis (TGA). Raman spectroscopy analyses of GO and PAO/rGO composites were mounted by using a LabRam HR Raman spectrometer (Horiba Jobin Yvon, France) at the excitation of 514.5 nm by Ar^+ laser. The XPS spectroscopy measurements were performed with an ESCALab220i-XL surface microanalysis system (VG Scientific, USA) equipped with an Al Kα ($h\nu$ = 1486.6 eV) source at a chamber pressure of 3×10^{-9} mbar. The surface-charging effects were corrected with C 1s peak at 284.4 eV as a reference. The TGA curves were examined with a Shimadzu TGA-50 thermogravimetric analyzer (Shimadzu, Japan) from room temperature to 800 °C at the heating rate of 10 °C/min with a nitrogen rate of 50 mL/min.

2.3 Adsorption of UO_2^{2+} on PAO/rGO composites and rGO

The adsorption property of UO_2^{2+} on PAO/rGO composites, PAO and rGO were studied at 20 ± 1 °C by batch adsorption technique. The suspensions of adsorbents and salinity solutions (e.g., NaCl) were mixed and shaken for 24 h to achieve the desired ionic strength and to guarantee the pre-equilibrium of salt with solid. Then UO_2^{2+} stock solution was added, and the pH of the suspensions were adjusted to the desired value by adding negligible amounts of 0.1 or 0.01 mol/L corresponding acid and basic solutions (e.g., HCl and NaOH). After the suspensions were shaken for 48 h, the adsorbents were separated from the liquid phase by centrifugation at 18000 r/min for 30 min (BECKMAN COULTER 64R, USA) at the same controlled temperature as the sorption experiments; next, the supernatants were filtered through 0.45 μm membrane filters. The residual UO_2^{2+} concentration in the supernatants was determined by inductively coupled plasma-atomic emission spectrometry (ICP-AES, Thermo Elemental, USA). All of the experimental data were the average of triplicate measurements; the average uncertainties were < 5%.

For the accurate determination of extremely low UO_2^{2+} (< 0.1 mg/L), UO_2^{2+} was extracted by tributyl phosphate (TBP) from its supernatant after filtration. Briefly, the pH of solution after filtration was adjusted to 2 with 6 mol/L HNO_3. Then UO_2^{2+} was extracted from the acidic solution by using 30% TBP in kerosene. Last, the UO_2^{2+} was back-extracted with water from the organic phase.

2.4 Regeneration-reuse of PAO/rGO composites

We selected HCl solution as eluent for the regeneration of the PAO/rGO composites. After adsorption with UO_2^{2+}, ~100 mg of 2.0PAO/rGO was shaken in different HCl solutions at 20 °C for 2 h to screen the concentration of HCl solutions.

Next, ~100 mg of PAO/rGO composites after UO_2^{2+} adsorption were thoroughly washed with the selected HCl solution and Milli-Q water until UO_2^{2+} was not detected in the aqueous solution. After that, the PAO/rGO composites were oven dried at 50 °C for one week to obtain the regenerated PAO/rGO composites, which were reused in the following experiments.

3 Results and discussion

3.1 Adsorbent characterization

The prepared PAO/rGO composites were characterized by Raman spectroscopy, X-ray photoelectron spectroscopy (XPS), thermogravimetric analysis (TGA), and scanning electron microscopy (SEM).

Raman spectroscopy technique, which can provide qualitative information about the surface functionalization of carbon-based materials, was employed to study the disorder degree of PAO/rGO composite surfaces. As can be seen from Figure 1, the Raman spectra of rGO and PAO/rGO composites are composed of two major characteristic peaks at ~1347 (D band) and ~1582 cm^{-1} (G band), which correspond to the vibration of disordered structure (e.g., the defects in the curved graphite sheet, sp^3 carbon, and/or other impurities) and the vibration of sp^2-hybridized carbon atoms, respectively. Comparing to the G band of GO at ~1612 cm^{-1}, a ~30 cm^{-1} significant decrease can be found in the G band of rGO and PAO/rGO composites at ~1584 cm^{-1}. This phenomenon can be assigned to the reduction of GO by NH_2OH. Zhao *et al.* [21] reported that NH_2OH can reduce GO to graphene and found that the G band decreased from ~1600 to ~1586 cm^{-1}. The peak-intensity ratio of D band to G band (I_D/I_G) is usually used to evaluate the degree of edge roughness and structural defect of carbon-based materials. Compared to the I_D/I_G value of GO (~1.00), the I_D/I_G value of rGO was increased to ~1.42 after NH_2OH treatment. This results means that the NH_2OH can successfully reduce GO to rGO. However, compared to the I_D/I_G value of rGO (~1.42), the I_D/I_G values of PAO/rGO composites were decreased to 1.04–1.16, which suggests that the formed PAO on PAO/rGO composite surfaces mainly existed in the form of amorphous carbon materials. We have previously found that the modification of multiwalled carbon nanotubes (MWCNTs) with special functional groups, such as poly(aniline) [22], poly(methylmethacrylate) [23], and β-cyclodextrin [24], increased the disorder degree of MWCNTs.

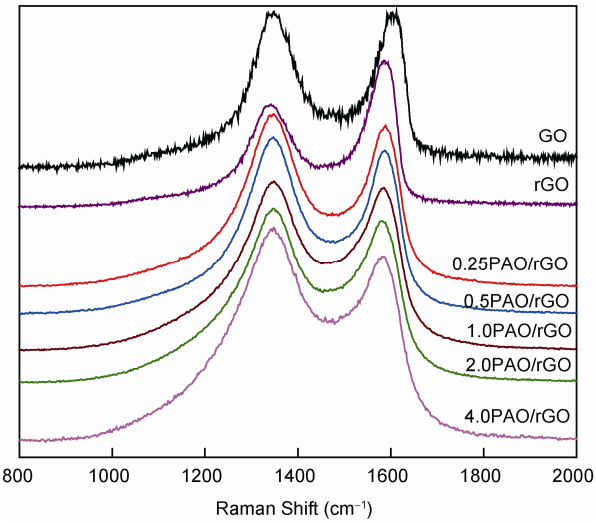

Figure 1 Raman spectra of GO, rGO, and PAO/rGO composites.

In XPS, the reduction of GO to rGO and the introduction PAO on rGO surface was observed as a lower energy shift of the C 1s spectrum between GO and PAO/rGO composites (Figure 2(a)), which was further confirmed by the deconvolution results (Table 1). The XPS C 1s spectra of GO and PAO/rGO composites can be deconvoluted into five components. The peaks at 284.6 ± 0.2 and 285.8 ± 0.2 eV corresponded to the sp^2 hybridized graphite-like carbon atoms (C=C) and sp^3-hybridized carbon atoms (C–C), respectively. The peaks at 286.7 ± 0.2, 287.4 ± 0.2, and 288.8 ± 0.2 eV were assigned, to the C–O single bonds, ethers, or alcohols; C=O double bonds such as aldehyde or ketone; and C(=O)OR as ester or carboxylic, respectively. In addition, abundant oxygen-containing carbon species in GO were reduced to C=C in PAO/rGO composites, which indicated the success reduction of GO to rGO under the amidoximation condition.

The XPS N 1s spectra intensities of PAO/rGO composites were proportional to the content of PAO (Figure 2(b)), and can be deconvoluted into three components (Table 2). The two typical peaks of PAO were found at 399.4 ± 0.2 and 400.2 ± 0.2 eV, which were assigned to N≡C–CH/NH_2–C=N–OH and H_2N–C=NOH, respectively [25]. The new peak at 401.5 ± 0.2 eV may be attributed to the positively charged nitrogen atoms [25, 26]. The amidoximation degree of PAO/rGO composites can be semi-quantita- tively determined by the integration area of oxime N 1s signal at 400.2 ± 0.2 eV to the area of N 1s signal at 399.4 ± 0.2 eV [25]. The calculated results gave similar amidoximation degrees of PAO/rGO composites, indicating the effectively conversion of poly(acrylonitrile) to PAO.

Surface topology is one of the important factors that affect the adsorption capacities of PAO/rGO composites. We investigated the reaction condition-surface topology relationships for PAO/rGO composites by SEM (Figure 3). The synthesized rGO nanosheets presented a smooth surface

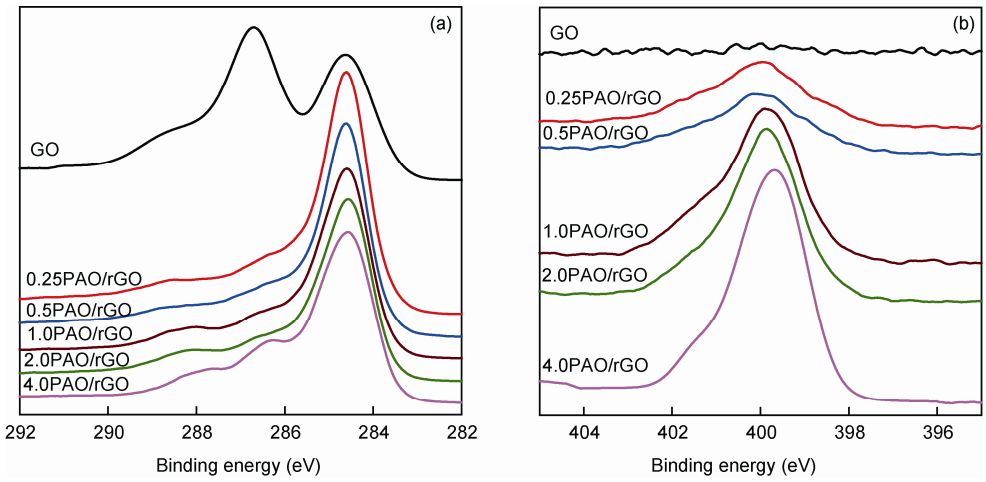

Figure 2 XPS C 1s spectra (a) and N 1s spectra (b) of GO and PAO/rGO composites.

Table 1 Curve-fitting results of XPS C 1s spectra

	Peak	BE [a)] (eV)	FWHM [b)] (eV)	Relative fraction (%)
GO	C=C	284.61	1.45	40.0
	C–C	285.90	0.75	2.05
	–C–OH	286.64	1.18	31.0
	>C=O	287.36	2.00	20.2
	$–COO^-$	288.80	1.46	6.78
0.25PAO/rGO	C=C	284.61	1.19	69.1
	C–C	285.84	0.92	9.25
	–C–OH	286.60	0.90	5.14
	>C=O	287.38	1.77	6.76
	$–COO^-$	288.72	1.93	9.76
0.5PAO/rGO	C=C	284.62	1.16	67.6
	C–C	285.80	1.00	9.21
	–C–OH	286.60	1.11	7.04
	>C=O	287.50	2.15	8.34
	$–COO^-$	288.79	2.20	7.86
1.0PAO/rGO	C=C	284.59	1.20	63.0
	C–C	285.71	1.26	16.3
	–C–OH	286.60	0.82	3.50
	>C=O	287.50	2.13	11.9
	$–COO^-$	288.70	1.49	5.28
2.0PAO/rGO	C=C	284.56	1.20	63.0
	C–C	285.70	1.21	14.6
	–C–OH	286.60	0.79	3.57
	>C=O	287.50	2.05	12.3
	$–COO^-$	288.70	1.74	6.54
4.0PAO/rGO	C=C	284.58	1.29	62.7
	C–C	285.90	1.29	16.0
	–C–OH	286.60	0.70	3.13
	>C=O	287.50	2.13	18.0
	$–COO^-$	288.70	1.00	0.19

a) Binding energy; b) full width at half-maximum.

morphology, like that of GO sheets, with a size of several micrometers (Figure 3(a)). Due to the decrease of hydrophilic property [27], the rGO sheets were agglomerated and accumulated, and presented layer-by-layer stacking microstructures. After being decorated with PAO, the surface of the rGO nanosheets became rough and shaggy, and showed hierarchical morphologies (Figure 3(b–f)), which indicated the nucleation and growth of PAO. Moreover, a continuous

Table 2 Curve-fitting results of XPS N 1s spectra

	Peak	BE (eV)	FWHM (eV)	Relative fraction (%)	*R* (H_2N–C=NOH/N≡C)
0.25PAO/rGO	N≡C	399.35	2.13	36.7	0.99
	H_2N–C=NOH	400.15	1.48	36.3	
	N^+	401.51	1.59	27.0	
0.5PAO/rGO	N≡C	399.40	1.37	43.7	0.97
	H_2N–C=NOH	400.20	1.37	42.3	
	N^+	401.53	1.30	14.0	
1.0PAO/rGO	N≡C	399.40	1.37	43.7	0.97
	H_2N–C=NOH	400.20	1.37	42.3	
	N^+	401.53	1.30	14.0	
2.0PAO/rGO	N≡C	399.40	1.50	43.1	0.96
	H_2N–C=NOH	400.10	1.34	41.2	
	N^+	401.43	1.47	15.7	
4.0PAO/rGO	N≡C	399.44	1.47	47.9	0.98
	H_2N–C=NOH	400.16	1.76	47.0	
	N^+	401.56	0.96	5.09	

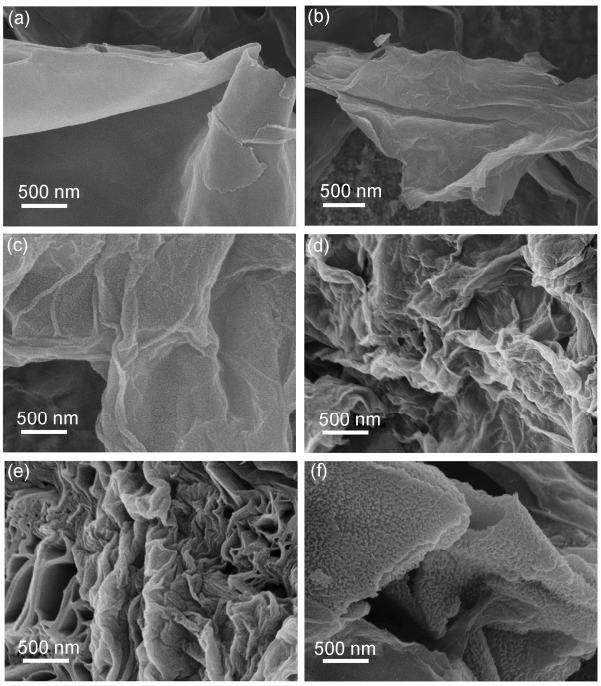

Figure 3 SEM images of (a) rGO, (b) 0.25PAO/rGO, (c) 0.5PAO/rGO, (d) 1.0PAO/rGO, (e) 2.0PAO/rGO, and (f) 4.0PAO/rGO.

increasing intensity of the wrinkle and entanglement was observed, with a high intensity at 2.0PAO/rGO and 4.0PAO/rGO.

We believed that acrylonitrile monomers would bind on the surfaces of the dispersed GO before polymerization. Once initiated by $(NH_4)_2S_2O_8$, acrylonitrile monomers began to polymerize and form many tiny and irregular protuberances on GO surfaces, which give a good dispersion status of PAO on GO surfaces. The polymerized poly(acrylonitrile) could function as new "active centers" for a further polymerization process to form porous microstructures, which provided convenient diffusion channels for metal ions (such as UO_2^{2+}) into the interior of adsorbent [27–29] and also improved its adsorption capacity. However, too much poly(acrylonitrile) in the formed pore and hole can reduce the pore size and/or even fill the pores of adsorbents (such as 4.0PAO/rGO), which would have an adverse effect on the interior diffusion of UO_2^{2+} in PAO/rGO composites and would reduce its adsorption capability.

TGA characterization is also carried out to detect the weight percent of PAO in PAO/rGO composites and to study the thermal stability of PAO/rGO composites. As can be seen from Figure 4, the weight losses of PAO/rGO composites increased with the increasing amounts of PAO. The notable weight loss of PAO/rGO composites from room temperature up to ~130 °C is related to the loss of moisture, which indicated the hydrophilicity of PAO/rGO composites. As depicted in Figure 4, the rGO prepared by NH_2OH of GO presents excellent thermal properties, such as pristine graphite [30, 31], and the significant weight loss of PAO/rGO composites in the temperature range of 130–800 °C are mainly attributed to the thermal decomposition and pyrolysis of PAO. After the decomposition temperature was increased to 700 °C, ~94.7% rGO [31] and only ~46.8% PAO [32] were retained in nitrogen condition. Therefore, the real weight ratio of PAO to rGO in PAO/rGO composites can be calculated as 0.25:1, 0.47:1, 1.00:1, 1.47:1, and 3.18:1 for 0.25PAO/rGO, 0.5PAO/rGO, 1.0PAO/rGO, 2.0PAO/rGO, and 4.0PAO/rGO, respectively. These results coincide well with the ratio of acrylonitrile monomer to GO at low acrylonitrile concentration, and lower than the ratio of acrylonitrile monomer to GO at high acrylonitrile concentration used in our experiment. This ratio is acceptable because high concentration of acrylonitrile monomer would be beneficial to the homogeneous nucleation of an acrylonitrile monomer, which would form random connections of acrylonitrile monomer in solution. Low concentrations of acrylonitrile

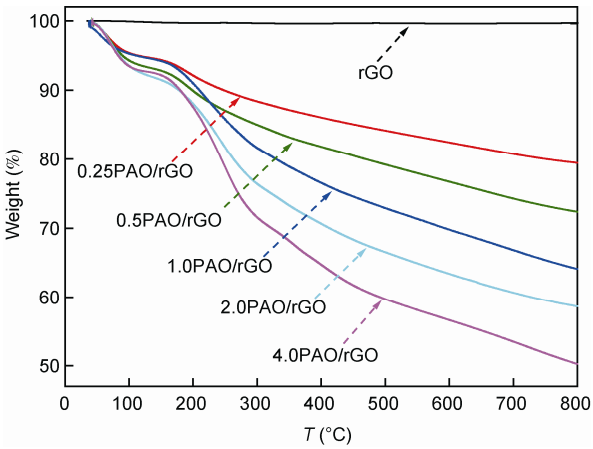

Figure 4 TGA curves of PAO/rGO composites.

monomer favor the heterogeneous nucleation of acrylonitrile monomer on GO nanosheets, which would form regularly aligned poly(acrylonitrile) on GO nanosheets. Our TGA results indicate that the amount of PAO in PAO/rGO composites could be adjusted simply by changing the mass ratio of acrylonitrile monomer to GO during the fabrication processes.

3.2 Adsorption of UO_2^{2+} on PAO/rGO composites

A comparison of the adsorption abilities of rGO, PAO, and different PAO/rGO composites as a function of UO_2^{2+} concentration, salinity, pH, and adsorbent content were carried out and studied with a batch adsorption technique. The adsorption isotherms were collected with a contact time of 48 h, m/V = 0.05 g/L, pH 4.0 ± 0.1, C[NaCl] = 0.1 mol/L, and T = 20 ± 1 °C (Figure 5(a)). The adsorption capacities of PAO/rGO composites for UO_2^{2+} reached as high as 872 mg/g at pH 4.0. The adsorption data were simulated by the Langmuir and Freundlich models; the relative parameters calculated from the two models are listed in Table 3. The Langmuir model gave better correlation coefficients and matched the experimental data much better than the Freundlich model did. The applicability of the Langmuir model suggested that PAO/rGO composite surfaces were uniform and homogeneous for UO_2^{2+} adsorption, and that the adsorbed UO_2^{2+} ions would form a monolayer on the surface of PAO/rGO composites. The C_{smax} values of UO_2^{2+} on rGO, PAO, and 2.0PAO/rGO composites at pH 4.0 were calculated to be ~33, ~188, and ~896 mg/g, respectively, based on the Langmuir model. Although rGO demonstrated minimal adsorption ability for UO_2^{2+}, PAO gave very low adsorption ability, however, the adsorption ability of PAO/rGO composites for UO_2^{2+} increased rapidly with a maximum value at 2.0PAO/rGO. A further increment of PAO would dramatically decrease its adsorption ability, which can be interpreted as the steric hindrance effect (morphology) as shown in SEM images. The adsorption process usually includes three stages: (1) external diffusion of contaminants from aqueous solutions to the external surface of the adsorbent; (2) interior diffusion of contaminants into the interior surface of the adsorbent; and (3) intrinsic complexation of contaminants with the active sites of the adsorbent [33, 34]. Considering that 2.0PAO/rGO presents a maximum intensity of the wrinkle and entanglement (Figure 3), the steric hindrance (morphologies) of PAO/rGO composites would affect the diffusion of UO_2^{2+}. This means that the accumulated, thick PAO layer (such as in 4.0PAO/rGO) would result in poor adsorption capability, as confirmed in our adsorption study. Similar effects were observed in our previous work on multiwalled carbon nanotubes, for example metal ions (Pb^{2+}) [35] and organic contaminants (polychlorinated biphenyls) [24].

Similar adsorption conditions were also applied to synthesized nanomaterials and traditional adsorbents. None gave adsorption abilities comparable to PAO/rGO for UO_2^{2+},

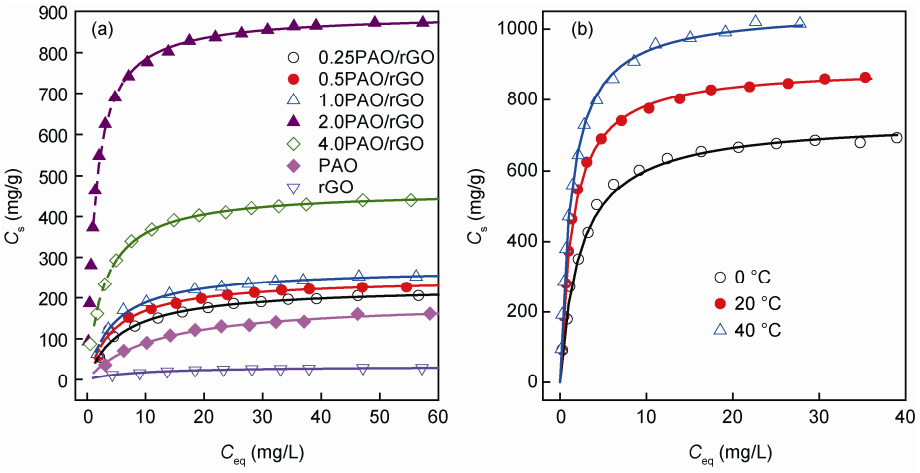

Figure 5 Adsorption isotherms of UO_2^{2+} ions from aqueous solutions on PAO/rGO composites. Contact time = 48 h, m/V = 0.05 g/L, pH 4.0 ± 0.1, C[NaCl] = 0.1 mol/L. (a) T = 20 ± 1 °C; (b) 2.0PAO/rGO.

which indicated the strong selectivity for PAO/rGO composites. Under optimized adsorption conditions, 2.0PAO/rGO composite was selected as the representive material for our study of the effect of environmental salinity on UO_2^{2+} adsorption.

Three different temperatures, 0, 20 and 40 °C, were selected to evaluate the impaction of environmental temperature for UO_2^{2+} extraction upon the adsorption isotherms (Figure 5). It can be seen that the adsorption ability increased at higher temperatures. The related thermodynamic parameters calculated from the temperature-dependent isotherms are listed in Table 4. The positive values of standard enthalpy changes (ΔH^0) indicated an endothermic process for the adsorption of UO_2^{2+} on 2.0PAO/rGO composite that was consistent with our observed results and the literature [15, 16, 36]. The negative values of Gibbs free energy change (ΔG^0) indicated that UO_2^{2+} adsorption on 2.0PAO/rGO was a spontaneous process [37]. The positive values of the entropy change (ΔS^0) reflected the strong affinity of 2.0PAO/rGO with UO_2^{2+}.

Salinity is also a critical environmental factor that affects the extraction of UO_2^{2+} from seawater because of the possible competitive adsorptions of other coexisting cations. However, PAO can highly adsorb UO_2^{2+} from other metal ions. Bilba *et al*. [38] reported that PAO had no affinity for most common cations in aqueous solutions, such as Na^+, K^+, Ca^{2+}, and Mg^{2+}. Rivas *et al*. [39] prepared PAO-chelating resin that exhibited excellent affinity for UO_2^{2+} in the presence of other metal ions. The salinity of wastewater is usually > 0.4 g/kg; for seawater the usual salinity is 36–38 g/kg. We selected cations as well as Na^+, K^+, Ca^{2+} and Mg^{2+} as the coexisting cations to investigate the adsorption efficiencies of 2.0PAO/rGO composites. The concentration of the coexisting cations ranged within 0.001–0.75 mol/L, which is about 5–3570 times higher than for UO_2^{2+}. As depicted in Figure 6, the 2.0PAO/rGO composite presented excellent tolerance to Na^+ and K^+, whereas, slightly reduced adsorption efficiency was observed for Ca^{2+} and Mg^{2+}; the latter was attributed to the ternary complexes formed by UO_2^{2+} and CO_3^{2-} with Mg^{2+} and Ca^{2+} [40, 41]. It is also noteworthy that the salinity we studied included most real salinities in aqueous solutions, which reveals that PAO/rGO composites can be used as promising adsorbents to extract large amounts of trace UO_2^{2+} ions from seawater.

We know that pH value is one of the most important environmental factors that controls the preconcentration and separation of UO_2^{2+} from aqueous solutions. As can be seen from Figure 6(b), the adsorption of UO_2^{2+} on PAO/rGO composites was strongly pH-dependent and rapidly increased with increasing pH values from ~2.0 to ~6.5. This result suggests that the adsorption of UO_2^{2+} on PAO/rGO composites is affected by the hydrolysis of UO_2^{2+} ions and the protonation-deprotonation of PAO in aqueous solutions. Barber *et al*. [18] and Zhang *et al*. [28, 29] reported that PAO is normally protonated in acidic solution, and that the protonation-deprotonation of PAO and the hydrolysis of UO_2^{2+} ions in aqueous solution are important factors that affect the adsorption of UO_2^{2+}on PAO-containing materials.

3.3 Regeneration-reuse of PAO/rGO composites

The regeneration-reuse property of PAO/rGO composites was also investigated for potential commercial applications. The regeneration was usually processed by eluting with different acidic or basic solutions, such as HCl [42], HNO_3 [42, 43], H_2SO_4 [39, 42], and Na_2CO_3 [39]. Herein, HCl was selected to regenerate 2.0PAO/rGO due to its quantitative efficiency to elute UO_2^{2+} [42]. The desorption efficiency compared to C_{HCl} is shown in Figure 7(a), which clearly illustrates that 0.1 mol/L HCl can remove UO_2^{2+} in nearly

Table 3 Experimental saturated adsorption capacity (Sat. C_s), Langmuir parameters and Freundlich model for UO_2^{2+}adsorption on rGO, PAO, and PAO/rGO composites at 20 ± 1 °C

Adsorbents	Sat. C_s (mg/g)	Langmuir model			Freundlich model		
		C_{smax} (mg/g)	b (L/mg)	R^2	K(mg/g)	1/n	R^2
0.25PAO/rGO	206	229	0.167	0.996	61.8	3.00	0.948
0.5PAO/rGO	227	249	0.211	0.984	76.4	3.24	0.917
1.0PAO/rGO	253	274	0.223	0.990	86.0	3.26	0.907
2.0PAO/rGO	872	896	0.709	0.994	374	3.21	0.900
4.0PAO/rGO	439	464	0.341	0.996	172	3.64	0.920
rGO	29	33	0.120	0.989	7.83	2.83	0.958
PAO	161	188	0.0926	0.993	32.0	2.32	0.946

Table 4 Thermodynamic parameters for UO_2^{2+} adsorption on 2.0PAO/rGO

T (°C)	lnK^0 (mL/g)	ΔG^0 (kJ/mol)	ΔH^0 (kJ/mol)	ΔS^0 (J/(mol K))
0	12.2	–27.7		
20	12.7	–31.0	14.2	154
40	13.0	–33.8		

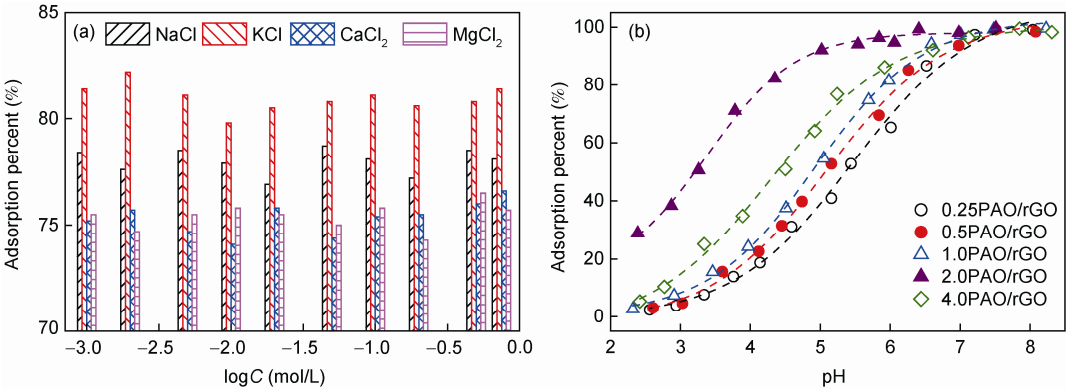

Figure 6 Effect of (a) salinity and (b) pH on the extraction of UO_2^{2+} ions from aqueous solutions on 2.0PAO/rGO. T = 20 ± 1 °C, contact time = 48 h, $C[UO_2^{2+}]_{initial}$ = 50.0 mg/L, m/V = 0.050 g/L. (a) pH 4.0 ± 0.1; (b) C[NaCl] = 0.1 mol/L.

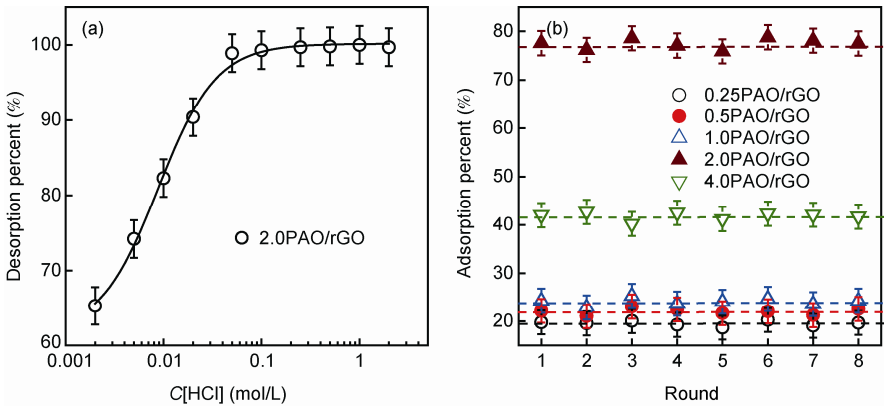

Figure 7 (a) Regeneration of 2.0PAO/rGO after UO_2^{2+} adsorption in HCl solution and (b) the recycling of 2.0PAO/rGO composites in the extraction of UO_2^{2+} from aqueous solutions. T = 20 ± 1 °C. (a) Contact time = 2 h; (b) contact time = 48 h, $C[UO_2^{2+}]_{initial}$ = 50.0 mg/L, m/V = 0.05 g/L, pH 4.0 ± 0.1, C[NaCl] = 0.1 mol/L.

quantitative yield. The adsorption efficiencies of the regenerated PAO/rGO composites for UO_2^{2+}, which stayed nearly the same even after 8 recycles (Figure 7(b)), are also promising. This easy adsorption-desorption cycle showed promising potential applications of PAO/rGO composites for the high extraction of trace UO_2^{2+} ions from large volumes of aqueous solutions.

3.4 Real application of PAO/rGO composites to extract μg/L level UO_2^{2+} from seawater

The real application of PAO/rGO composites in the extraction of naturally occurring UO_2^{2+} from seawater is shown in Table 5. A contaminated mg/L level UO_2^{2+} water from the Yangtze River (5–0 mg/L UO_2^{2+}, m/V = 0.050 g/L, pH 7.5–4.0) was adsorbed by 2.0PAO/rGO with high adsorption efficiencies of 77%–99%. With this promising result, lower μg/L-level-contaminated (10–1000 μg/L UO_2^{2+}, m/V = 0.050 g/L, pH 8.2) UO_2^{2+} water from East China Sea was collected for further investigation. A slightly lower efficiency was obtained for 2.0PAO/rGO in the range of 67%–86%. Finally, this adsorption method was applied to naturally occurring UO_2^{2+} (3.2 μg/L UO_2^{2+}, m/V = 0.050 g/L, pH 8.2) seawater (East China Sea). An amazing result was achieved with an efficiency of 65%, which strongly encourages the direct applications of the PAO/rGO composites in UO_2^{2+} extraction from seawater.

4 Conclusions

PAO was successfully introduced onto an rGO surface by using *in situ* polymerization of acrylonitrile monomer and subsequent amidoximation with hydroxylamine. The results of batch adsorption experiments revealed that the PAO/rGO composites can highly adsorb trace level UO_2^{2+} ions from aqueous solution in the presence of other cations. The adsorption abilities to UO_2^{2+} ions were pH-dependent and the adsorption process was found to be endothermic and spontaneous. These results make PAO/rGO a potential adsorbent for UO_2^{2+} extraction from seawater.

Table 5 Selected extraction results of UO_2^{2+} from aqueous solutions with 2.0PAO/rGO

Sample	Salinity	pH	*m*/*V* (g/L)	$C[UO_2^{2+}]$ (μg/L)		Adsorption (%)
				Initial	Final	
Yangtze River water	Na^+ (8.7 mg/L), K^+ (2.0 mg/L), Ca^{2+} (39.2 mg/L), Mg^{2+} (9.7 mg/L), Cl^- (12.1 mg/L), and SO_4^{2-} (32.2 mg/L)	7.5	0.050	50000	152	99.7
		6.4	0.050	50000	353	99.3
		5.5	0.050	50000	2952	94.1
		4.4	0.050	50000	8870	82.3
		4.0	0.050	50000	11500	77.0
		4.0	0.050	25000	1370	94.5
		4.0	0.050	10000	452	95.5
		4.0	0.050	5000	226	95.5
Seawater [a)]	Na^+ (11.0 g/L), K^+ (0.364 g/L), Ca^{2+} (0.419 g/L), Mg^{2+} (1.33 g/L), Cl^- (19.8 g/L), and SO_4^{2-} (2.77 g/L)	8.2	0.050	1000	138	86.2
		8.2	0.050	200	42.4	78.8
		8.2	0.050	50	10.9	78.2
		8.2	0.050	10	3.27	67.3
		8.2	0.050	3.2	1.13	64.8

a) The seawater obtained from East China Sea was added to different amounts of UO_2^{2+} intentionally. The pH values of the suspensions were kept at the initial pH value (8.2) by negligible amounts of 0.1 or 0.01 mol/L NaOH solutions.

This work was supported by the Chinese National Fusion Project for ITER (2013GB110005), the National Natural Science Foundation of China (91326202, 21207136, 21272236, 21225730), the Priority Academic Program Development of Jiangsu Higher Education Institutions, the Collaborative Innovation Center of Radiation Medicine of Jiangsu Higher Education Institutions, Hefei Center for Physical Science and Technology (2012FXZY005), and the Science Foundation of Institute of Plasma Physics (DSJJ-13-YY01).

1 Manos MJ, Kanatzidis MG. Layered metal sulfides capture uranium from seawater. *J Am Chem Soc*, 2012, 134: 16441–16446
2 Shao D, Jiang Z, Wang X, Li J, Meng Y. Plasma induced grafting carboxymethyl cellulose on multiwalled carbon nanotubes for the removal of UO_2^{2+} from aqueous solution. *J Phys Chem B*, 2009, 113: 860–864
3 Ren X, Yang S, Tan X, Chen C, Wang X. Investigation of radionuclide Co(II) binding to TiO_2 by batch technique, surface complexation model and DFT calculations. *Sci China Chem*, 2012, 55: 1752–1759
4 Wang X, Yuan L, Wang Y, Li Z, Lan J, Liu Y, Feng Y, Zhao Y, Chai Z, Shi W. Mesoporous silica SBA-15 functionalized with phosphonate and amino groups for uranium uptake. *Sci China Chem*, 2012, 55: 1705–1711
5 Wu Y, Mimura H, Niibori Y, Ohnishi T, Koyama S, Wei Y. Study on adsorption behavior of cesium using ammonium tungstophosphate (AWP)-calcium alginate microcapsules. *Sci China Chem*, 2012, 55: 1719–1725
6 Yang S, Sheng G, Guo Z, Tan X, Xu J, Wang X. Investigation of radionuclide ^{63}Ni(II) sequestration mechanisms on mordenite by batch and EXAFS spectroscopy study. *Sci China Chem*, 2012, 55: 632–642
7 Shao D, Xu D, Wang S, Fang Q, Wu W, Dong Y, Wang X. Modeling of radionickel sorption on MX-80 bentonite as a function of pH and ionic strength. *Sci China Chem*, 2009, 52: 362–371
8 Usuda S, Wei Y, Liu R, Li Z, Xu Y, Wu Y, Kim S. Challenges to develop single-column MA(III) separation from HLLW using R-BTP type adsorbents. *Sci China Chem*, 2012, 55: 1732–1738
9 Wei Y, Wang X, Liu R, Wu Y, Usuda S, Arai T. An advanced partitioning process for key elements separation from high level liquid waste. *Sci China Chem*, 2012, 55: 1726–1731
10 Yusan SD, Akyil S. Sorption of uranium(VI) from aqueous solutions by akaganeite. *J Hazard Mater*, 2008, 160: 388–395
11 Li J, Guo Z, Zhang S, Wang X. Enrich and seal radionuclides in magnetic agarose microspheres. *Chem Eng J*, 2011, 172: 892–897
12 Sather AC, Berryman OB, Rebek J Jr. Selective recognition and extraction of the uranyl ion. *J Am Chem Soc*, 2010, 132: 13572–13574
13 Praveen RS, Metilda P, Daniel S, Rao TP. Solid phase extractive preconcentration of uranium(VI) using quinoline-8-ol anchored chloromethylated polymeric resin beads. *Talanta*, 2005, 67: 960–967
14 Romanchuk AY, Slesarev AS, Kalmykov SN, Kosynkinz DV, Tour JM. Graphene oxide for effective radionuclide removal. *Phys Chem Chem Phys*, 2013, 15: 2321–2327
15 Liu X, Liu H, Ma H, Cao C, Yu M, Wang Z, Deng B, Wang M, Li J. Adsorption of the uranyl ions on an amidoxime-based polyethylene nonwoven fabric prepared by preirradiation-induced emulsion graft polymerization. *Ind Eng Chem Res*, 2012, 51: 15089–15095
16 Das S, Pandey AK, Athawale AA, Manchanda VK. Exchanges of uranium(VI) species in amidoxime-functionalized sorbents. *J Phys Chem B*, 2009, 113: 6328–6335
17 Lutfor MR, Silong S, Zin WM, Rahman MZA, Ahmad M, Haron J. Preparation and characterization of poly(amidoxime) chelating resin from polyacrylonitrile grafted sago starch. *Eur Polym J*, 2000, 36: 2105–2113
18 Barber PS, Kelley SP, Rogers RD. Highly selective extraction of the uranyl ion with hydrophobic amidoxime-functionalized ionic liquids via η^2 coordination. *RSC Adv*, 2012, 2: 8526–8530
19 Zhou X, Zhang J, Wu H, Yang H, Zhang J, Guo S. Reducing graphene oxide via hydroxylamine: a simple and efficient route to graphene. *J Phys Chem C*, 2011, 115: 11957–11961
20 Mao S, Yu K, Cui S, Bo Z, Lu G, Chen J. A new reducing agent to prepare single-layer, high-quality reduced graphene oxide for device applications. *Nanoscale*, 2011, 3: 2849–2853
21 Zhao X, Zhou S, Shen Q, Jiang LP, Zhu JJ. Fabrication of glutathione photoelectrochemical biosensor using graphene-CdS nanocomposites. *Analyst*, 2012, 137: 3697–3703
22 Shao D, Hu J, Chen C, Sheng G, Ren X, Wang X. Polyaniline multiwalled carbon nanotube magnetic composite prepared by plasma-induced graft technique and its application for removal of aniline and phenol. *J Phys Chem C*, 2010, 114: 21524–21530
23 Shao D, Hu J, Jiang Z, Wan X. Removal of 4,4′-dichlorinated biphenyl from aqueous solution using methyl methacrylate grafted multiwalled carbon nanotubes. *Chemosphere*, 2011, 82: 751–758
24 Shao D, Sheng G, Chen C, Wang X, Nagatsu M. Removal of polychlorinated biphenyls from aqueous solutions using β-cyclodextrin grafted multiwalled carbon nanotubes. *Chemosphere*, 2010, 79: 679–685
25 Yu ZJ, Kang ET, Neoh KG. Amidoximation of the acrylonitrile polymer grafted on poly(tetrafluoroethylene-*co*-hexafluoropropylene) films and its relevance to the electroless plating of copper. *Langmuir*,

2002, 18: 10221–10230
26 Wu G, Li L, Li JH, Xu BQ. Polyaniline-carbon composite films as supports of Pt and PtRu particles for methanol electrooxidation. *Carbon*, 2005, 43: 2579–2587
27 Pan Y, Bao H, Li L. Noncovalently functionalized multiwalled carbon nanotubes by chitosan-grafted reduced graphene oxide and their synergistic reinforcing effects in chitosan films. *ACS Appl Mater Interf*, 2011, 3: 4819–4830
28 Zhang A, Asakura T, Uchiyama G. The adsorption mechanism of uranium(VI) from seawater on a macroporous fibrous polymeric adsorbent containing amidoxime chelating functional group. *React Funct Polym*, 2003, 57: 67–76
29 Zhang A, Uchiyama G, Asakura T. PH effect on the uranium adsorption from seawater by a macroporous fibrous polymeric material containing amidoxime chelating functional group. *React Funct Polym*, 2005, 63: 143–153
30 Kamada S, Nomoto H, Fukuda K, Fukawa T, Shirai H, Kimura M. Noncovalent wrapping of chemically modified graphene with π-conjugated disk-like molecules. *Colloid Polym Sci*, 2011, 289: 925–932
31 Shen J, Hu Y, Shi M, Lu X, Qin C, Li C, Ye M. Fast and facile preparation of graphene oxide and reduced graphene oxide nanoplatelets. *Chem Mater*, 2009, 21: 3514–3520
32 Joseph P, Tretsiakova-Mcnally S. Combustion behaviours of chemically modified polyacrylonitrile polymers containing phosphorylamino groups. *Polym Degrad Stab*, 2012, 97: 2531–2535
33 Abdel-Aal SE, Gad YH, Dessouki AM. Use of rice straw and radiation-modified maize starch/acrylonitrile in the treatment of wastewater. *J Hazard Mater B*, 2006, 129: 204–215
34 Sheng G, Yang S, Sheng J, Hu J, Tan X, Wang X. Macroscopic and microscopic investigation of Ni(II) Sequestration on diatomite by Batch, XPS and EXAFS techniques. *Environ Sci Technol*, 2011, 45: 7718–7726
35 Shao D, Ren X, Hu J, Chen Y, Wang X. Preconcentration of Pb^{2+} from aqueous solution using poly(acrylamide) and poly(*N*,*N*-dimethylacrylamide) grafted multiwalled carbon nanotubes. *Colloid Surf A*, 2010, 360: 74–84
36 Das S, Pandey AK, Vasudevan T, Athawale AA, Manchanda VK. Adsorptive preconcentration of uranium in hydrogels from seawater and aqueous solutions. *Ind Eng Chem Res*, 2009, 48: 6789–6796
37 Song Q, Ma L, Liu J, Bai C, Geng J, Wang H, Li B, Wang L, Li S. Preparation and adsorption performance of 5-azacytosine-functionalized hydrothermal carbon for selective solid-phase extraction of uranium. *J Colloid Interf Sci*, 2012, 386: 291–299
38 Bilba D, Bilba N, Moroi G. Removal of mercury(II) ions from aqueous solutions by the polyacrylamidoxime chelating fiber. *Sep Sci Technol*, 2007, 42: 171–184
39 Rivas BL, Maturana HA, Villegas S. Adsorption behavior of metal ions by amidoxime chelating resin. *J Appl Polym Sci*, 2000, 77: 1994–1999
40 Phillips DH, Watson DB, Kelly SD, Ravel B, Kemner KM. Deposition of uranium precipitates in dolomitic gravel fill. *Environ Sci Technol*, 2008, 42: 7104–7110
41 Dong W, Brooks SC. Determination of the formation constants of ternary complexes of uranyl and carbonate with alkaline earth metals (Mg^{2+}, Ca^{2+}, Sr^{2+}, and Ba^{2+}) using anion exchange method. *Environ Sci Technol*, 2006, 40: 4689–4695
42 Preetha CR, Gladis JM, Rao TP, Venkateswaran G. Removal of toxic uranium from synthetic nuclear power reactor effluents using uranyl ion imprinted polymer particles. *Environ Sci Technol*, 2006, 40: 3070–3074
43 Coşkun R, Soykan C. Preparation of amidoximated polyester fiber and competitive adsorption of some heavy metal ions from aqueous solution onto this fiber. *J Appl Polym Sci*, 2009, 112: 1798–1807